

National University of Singapore
School of Computing
Dept. of Computer Science

Graduate Research Paper

**Segmentation of Vascular Structures from
Medical Images**

by

Qi Yingyi

Supervisor: Dr. Leow Wee Kheng (Associate Professor)

July, 2006

Abstract

Medical image segmentation is applied to extract vascular structures from various medical images, such as CT (Computed Tomography), MRI (Magnetic Resonance Imaging). In this paper, existing algorithms for vasculature segmentation are classified into several categories, and a thorough literature review is given to discuss their main ideas, pros and cons. Based on the review, some possible research topic is proposed. Some preliminary work is also presented. And the experimental results are discussed.

Contents

Contents	i
1 Introduction	1
1.1 Motivation	1
1.2 Definition of Segmentation Problem	3
1.3 Organization of the Paper	4
2 Existing Work	5
2.1 General Segmentation Algorithms	5
2.1.1 Thresholding	5
2.1.2 Region Growing	6
2.1.3 Watershed	7
2.1.4 Classification	10
2.1.5 Clustering	10
2.2 Model-based Approach	11
2.2.1 Deformable Models	12
2.2.2 Atlas-based Approach	16
2.3 Comparison of Segmentation Methods	17
2.4 Vascular Structure Segmentation Algorithms	18
2.4.1 Centerline Detection	18
2.4.2 Region Growing	19
2.4.3 Matched Filter	20
2.4.4 Deformable Model-based Approaches	20
2.4.5 Geometric Parametric Model-based Approach	22
2.4.6 Classification	24
2.4.7 Stochastic Approach	27
2.4.8 Summary	27
3 Possible Research Topics	31

3.1	Segmentation of Blood Vessels from Temporal Sequence of Angiograms	31
3.2	Segmentation and Annotation of Multiple Parts of 3-D Cardiac Vasculature	32
4	Preliminary Work	35
4.1	Characteristics of Input Images	35
4.2	Problem Description	35
4.3	Algorithm	37
4.3.1	Preprocessing	37
4.3.2	Level Set Evolution	39
4.3.3	Visualization	40
4.4	Experiments	40
5	Conclusion	45
	Bibliography	47

Chapter 1

Introduction

1.1 Motivation

Vascular structures are objects in the human body that have tree structures with lots of branches. Each branch often has a tubular shape. Vascular structures include blood vessels, neurovascular structures, vascular structures in livers, coronary artery, airway tree (pulmonary tree), colon, and nerve channels [38].

There are many diseases associated with the vascular structures listed above. For example, cancer cannot progress without the formation of new blood vessels to supply the malignant cells' metabolic demand. In coronary heart disease, inflamed fatty deposits in the blood vessel wall obstruct the coronary arteries which supply blood to the heart. This leads to narrowing of arteries called arterial stenosis. When the blockages become severe enough, blood flow to the heart is restricted. Then, the portion of the heart muscle supplied by the diseased arteries dies. If the affected area is large enough, the patient will die. Bronchiectasis is a chronic inflammatory or degenerative condition of one or more bronchi or bronchioles of the lungs, which suffer from dilation and loss of elasticity of the walls. This results in airflow obstruction and impaired clearance of secretions in the lungs.

Medical images, such as magnetic resonance (MR) images, computed tomography (CT) images, and angiograms, play an important role in diagnosis and treatment of diseases related to vascular structures. For example, blood vessels appear very clearly in x-ray angiograms and CT images (Figure 1.1) due to injected intravenous contrast agent. It is easy for doctors to observe narrowing, dilation or obstruction of vessels, which will lead to severe diseases.

Computer-aided diagnosis based on medical images is a very important

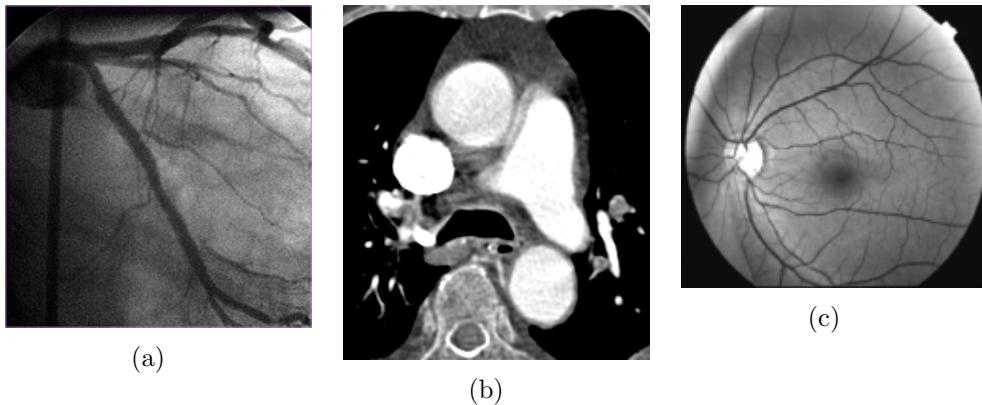


Figure 1.1: Images of vascular structures. (a) A cardiac angiogram showing cardiac blood vessels, (b) a CT image of the cross section of the cardiac blood vessels, and (c) a retinal fundus image showing the blood vessels on the retina.

technique that helps doctors detect diseases earlier. It can obtain the whole tree structure of blood vessels. It can compare the data extracted from a patient's image data with a corresponding model to increase the recognition accuracy of abnormalities of vascular structures.

Computer analysis of medical images can also be used for treatment. For example, qualitative and quantitative comparisons between sets of images of one patient at different time can provide evidence for the effects of medicine or treatment.

Computer analysis of medical images requires various medical image processing techniques. Among them, segmentation is usually the first step in processing medical images. It is also a crucial step that affects the accuracy of the final result in the application. For example, segmentation of blood vessels from 2-D or 3-D images should be accurate enough. Otherwise, subsequent steps based on the segmentation results, such as 3-D reconstruction, visualization, and quantification of the vessels, become error prone. Segmentation of vascular structures is a difficult task because vascular structures often have complex topological and geometric structures. Moreover, high-intensity noise in the images may confuse the segmentation algorithms.

1.2 Definition of Segmentation Problem

In general, the goal of segmentation is to partition an image I into several disjoint regions R_i such that each region is homogeneous with respect to some properties:

$$\begin{aligned}
 I &= \bigcup_{i=1}^N R_i & (1.1) \\
 R_i \cap R_j &= \emptyset \text{ for } i \neq j \\
 P(R_i) &\approx 1 \text{ for } i = 1, 2, \dots, N \\
 P(R_i \cup R_j) &\approx 0 \text{ for } i \neq j
 \end{aligned}
 \tag{1.2}$$

where the function $P(R) \in [0, 1]$ measures the homogeneity of the region. $P(R) = 1$ means the region is homogeneous, and $P(R) = 0$ means the region is inhomogeneous.

In particular, there are three variations to the vascular structure segmentation problem:

- 2-D structure from single 2-D image:
Given a 2-D image, group its pixels into two groups, i.e., the vascular structure and the background.
- 3-D structure from 3-D volumetric image:
3-D volumetric image consists of a set of consecutive 2-D slices. Similar to the 2-D case, the problem is to group all its voxels into two groups. Based on the segmentation result, a 3-D model of the vascular structure can be obtained.
- 2-D structure from 2-D temporal sequence:
This variation is to segment the 2-D vascular structure from a 2-D temporal sequence. Vascular structures move and change shape over time due to physiological activities, such as breathing and bumping of the heart. Some parts of the vessels may overlap others in some image frames. In some cases, such as angiograms, blood vessels may not be clearly visible in all image frames due to the flowing in and out of contrast agent along with the blood (Figure 1.2). Therefore, segmentation of all the blood vessels in all the image frame poses a great difficulty.

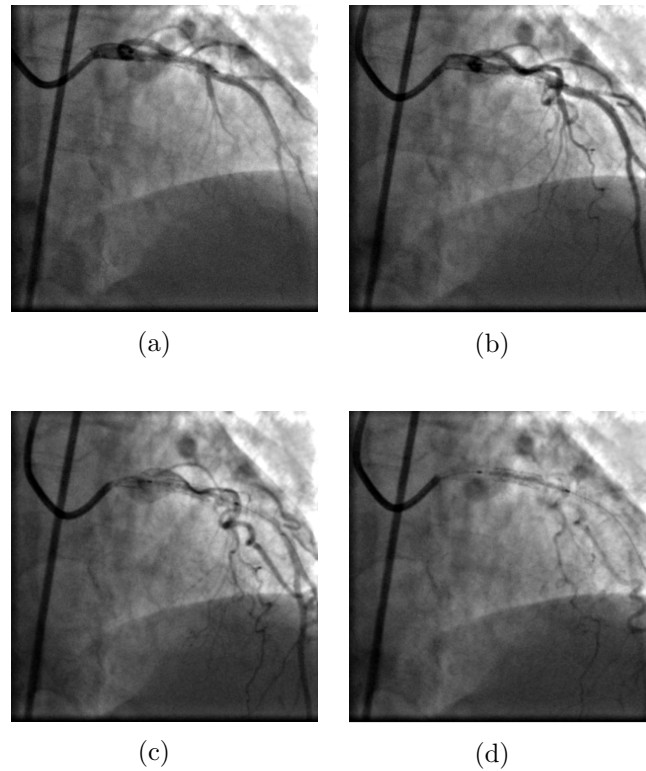


Figure 1.2: Example of 2-D temporal sequence of cardiac angiograms. Blood vessels change position, shape and intensity over time.

1.3 Organization of the Paper

In Section 2, general algorithms and model-based algorithms for the segmentation of medical images will be first discussed. Based on them, techniques that are specifically designed for vascular structure segmentation are covered in Section 2.4. From the literature review related to vascular structure segmentation, some possible research topics that deserve more emphases and research are discussed in Chapter 3. Preliminary segmentation results using existing algorithms are shown in Chapter 4. Finally, the paper concludes in Chapter 5.

Chapter 2

Existing Work

General segmentation algorithms can work well with simple biomedical images with homogeneous features (Section 2.1). However, by themselves, they may fail to segment complex images with inhomogeneous features. More sophisticated model-based algorithms are developed for segmenting complex images (Section 2.2). Specific algorithms for segmenting vascular structures are discussed in Section 2.4.

2.1 General Segmentation Algorithms

General algorithms for medical image segmentation can be divided into five categories: thresholding, region growing, watershed, classification and clustering.

2.1.1 Thresholding

Thresholding is one of the basic segmentation techniques. It segments an image by partitioning it into two parts depending on a threshold value that is related to the image intensities or other image features. In the case of multithresholding, more than one threshold can be used to segment an image into more than two parts.

There are two kinds of thresholding techniques: global thresholding and local thresholding. Global thresholding determines a single threshold based on the intensity histogram or other features of the entire image [34, 49]. Then image is divided into two regions, one with feature values greater than the threshold, and the other with feature values less than the threshold (Figure 2.1).

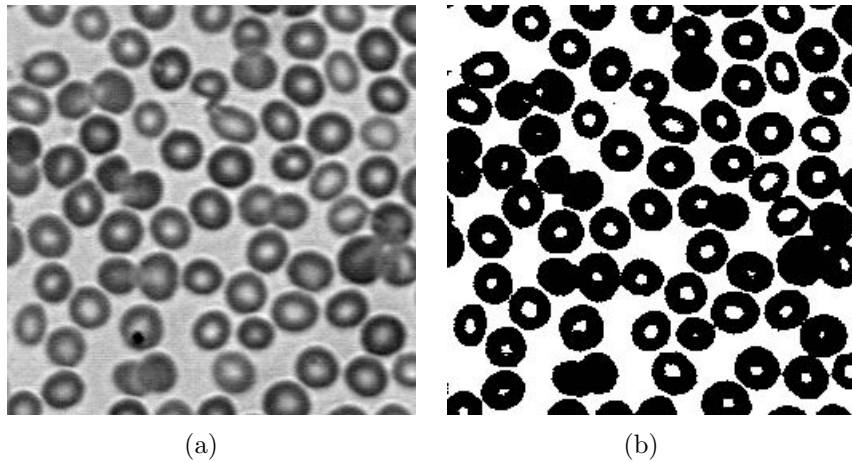


Figure 2.1: Example of thresholding result. (a) The input image, (b) the thresholding result.

In many applications, global thresholding cannot produce good segmentation results for complex images whose background may not have a constant intensity. One single threshold for an entire image might be inadequate. Therefore, local thresholding is often used. It determines local thresholds by splitting the image into subimages and computing thresholds for each subimage [12], or by examining the average image intensities or other statistics in the neighborhood of each pixel [7, 15, 40].

Thresholding is a simple and efficient segmentation method when the objects to be segmented have very contrasting intensities or features compared to the background. Usually this kind of methods ignores the shape features of an image, which makes thresholding techniques very sensitive to noise. Moreover, it often results in over-segmentation, i.e., the segmentation result contains many small regions, due to feature inhomogeneity.

2.1.2 Region Growing

Compared with thresholding, region growing is designed to look for groups of pixels with similar properties with respect to some predefined criteria. In the simplest form, it starts from one or more seed points that serve as the initial regions. Then, it adds neighboring pixels one at a time into the regions if they have similar intensities or other features based on some predefined similarity measures (Figure 2.2) [19, 57, 62].

Selections of seed points and similarity measure are the most important issues in region growing. Seed points can be chosen by some automatic procedures [57, 71, 79] or selected manually, especially for complex cases [62]. In general, points that are most representative of the desired regions are chosen as seed points. Different criteria are used according to different applications, for example, points with smallest gradient length [57], points located in a special position [79], and points with special texture information [71].

Similarity measure of intensity or other features should be determined carefully. If the similarity condition is too strict, it may result in over-segmentation. Otherwise, it may cause insufficient segmentation.

The primary disadvantage of region growing is that its result may vary according to the different seed points selected. Region growing can be very sensitive to noise, resulting in over-segmentation or insufficient segmentation. On the other hand, due to the neighbor growing scheme, region growing always generates connected regions. By starting from multiple seed points, it can group regions at different spatial locations with similar features into one group.

2.1.3 Watershed

Watershed segmentation utilizes image morphology. A gray-scale image is considered as a topographic surface with respect to intensity. In the gray-level profile of the image, local minima define catchment basins and local maxima define the watershed lines (Figure 2.3). Watershed algorithm requires at least one starting point for each desired object to be segmented, including the background as a separate object. These starting points are usually provided by some automatic procedures (Section 2.1.2). Then, the entire topographical surface is flooded as if water rises through the starting points. When water in distinct catchment basins is about to merge, a dam is built to prevent the merging. The flooding stops when only the tops of the dams are visible above the water line. These dams correspond to watershed lines [24].

Watershed algorithms always produce a complete division of the image. However, sometimes they can result in over-segmentation (Figure 2.4(b)) because noise in the image may form a lot of local minima. Moreover, they usually cannot be used to extract thin structures or structures with low signal-to-noise ratio [25].

In order to overcome these drawbacks, watershed algorithms are modified according to the characteristics of the input images [46, 68], or they are combined with other techniques, like region merging, to produce better results (Figure 2.4(c)) [28, 69].

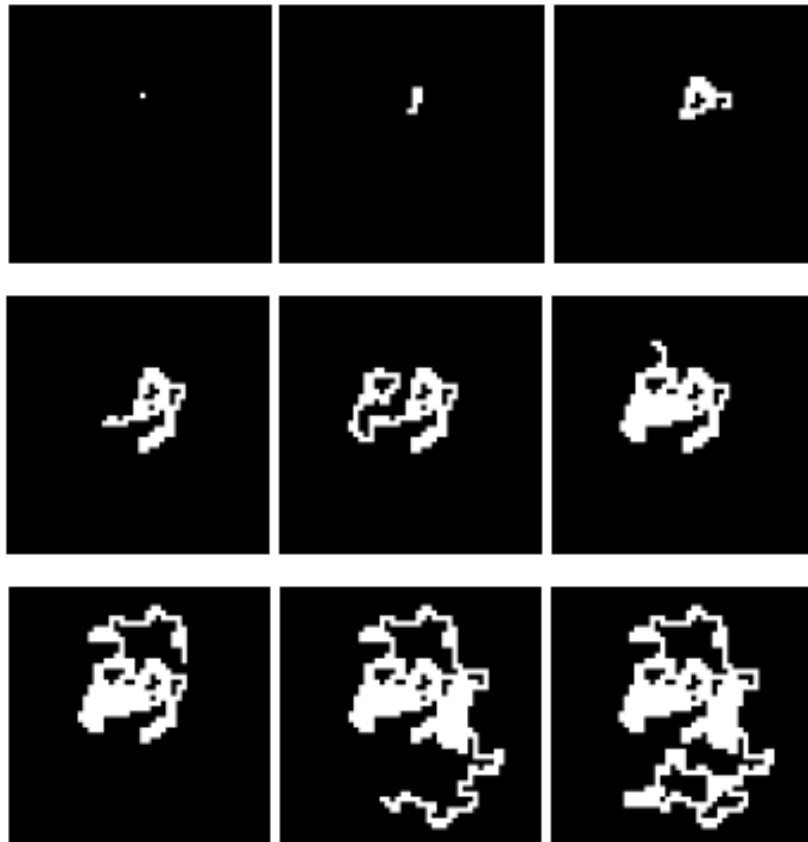


Figure 2.2: Randomized region growing after seed point setting and visiting 9, 40, 100, 150, 200, 300, 400 and 475 pixels [57].

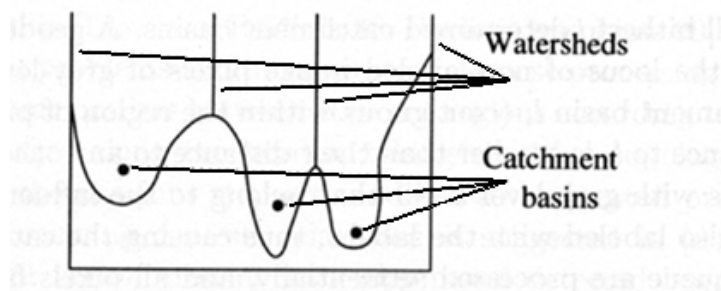
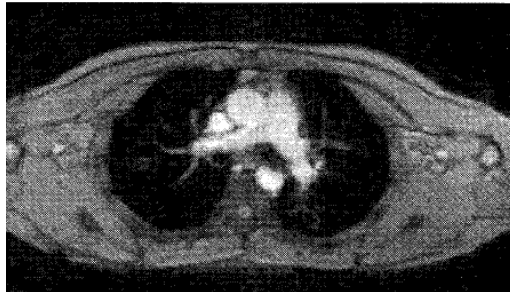
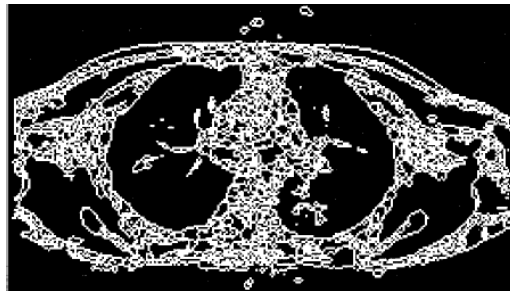


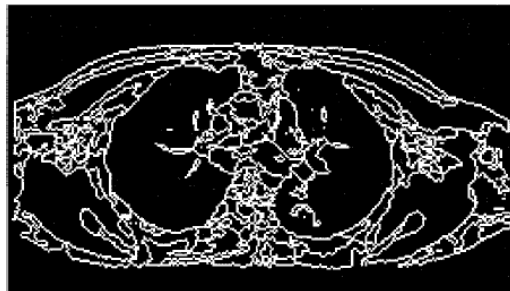
Figure 2.3: Catchment basin and watershed lines in watershed algorithms [72].



(a)



(b)



(c)

Figure 2.4: Image segmentation results using watershed and region merging [28]. (a) Raw MR image, (b) initial over-segmentation (3058 regions), and (c) improved segmentation result (40 regions).

2.1.4 Classification

Classification method classifies pixels into known classes based on one or more characteristics. It requires a training set of previously labeled pixels. There are two common steps among all the classification methods. One is to select some features according to the characteristics of the input image to form a multi-dimensional feature space. Each pixel or patch of pixels to be classified is represented as a feature vector in the feature space. Then, the similarity or closeness between the feature vectors can be described using some measures such as Euclidean distance. The other common step is to mark a subset of vectors with known class labels. Usually this step is performed manually. Finally for all the classification methods, the task is to determine a mapping function from each vector to one of the known classes using a training algorithm.

Various classifiers have been used to obtain the mapping function, e.g., linear classifiers [70], k-nearest-neighbor [16, 58], boosting [59], decision trees [35], neural networks [3, 18, 32, 52], support vector machines [60, 80], etc. For example, Kalinlin et al. segment different anatomical regions in abdominal CT using decision tree [35]. The feature used is based on pixel-wise Haralick co-occurrence texture features [27]. The classification result is post-processed by a median filter to improve the segmentation (Figure 2.5).

Classifiers can determine the classes of different regions in an image effectively, as long as the extracted features are sufficient to distinguish different classes. It may lead to biased results when a small set of training data is used [4]. If the features are based on a single pixel, then, the boundaries between segmented regions can be determined precisely. On the other hand, if the features are extracted from a neighborhood of pixels, the locations of the segmented region boundaries are uncertain. Another disadvantage of classification method is the requirement of manual work to prepare the training data, which is time-consuming and tedious.

2.1.5 Clustering

In clustering, a feature vector is extracted from each patch of pixels in the input image. It corresponds to a vector in the feature space. Then, clustering is performed to group the vectors of various patches into clusters such that vectors in each cluster have similar characteristics according to some predefined distance measure, and vectors in different clusters have different characteristics.

Clustering can be hierarchical or partitional. Hierarchical clustering can be agglomerative (bottom-up) or divisive (top-down). The former starts with each vector as a separate cluster and then merges them into larger

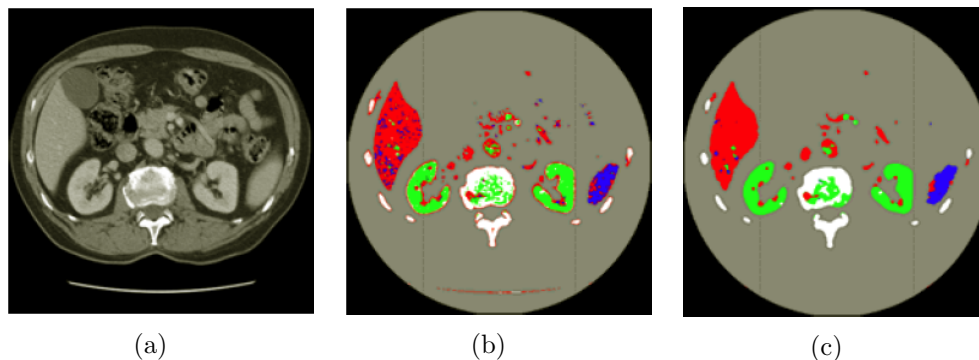


Figure 2.5: Segmentation by classification [35]. (a) Input CT image, (b) segmented result using classification, and (c) post-processed result using median filter.

clusters successively [33, 74], while the latter begins with the whole set of vectors as a single cluster and divides it into smaller clusters successively. Partitional algorithms includes k -means clustering [23] and its variations, such as fuzzy c -means algorithm [13, 54] (Figure 2.6).

In [23], k -means clustering is used in spatio-temporal segmentation of medical image sequence. In this approach segmentation is not done on a simple frame-by-frame basis but utilizes multiple image frames. Thus features, e.g. brightness and the Euclidean norm of the optical flow vector, are extracted from the actual image that has to be segmented and from neighboring image frames in the sequence. This scheme makes use of the motion of desired objects.

Like classification, clustering result is dependent on feature extraction. k -means clustering and its variations are sensitive to initialization. It is important to choose initial clusters carefully. In general, clustering does not take into account spatial information of the pixels or patches of pixels.

2.2 Model-based Approach

General segmentation algorithms typically require that the objects to be segmented are homogeneous with respect to some features, usually intensity. On the other hand model-based algorithms does not require the regions to be homogeneous because they make use of domain-specific prior information. There are mainly two kinds of models: deformable model and atlas.

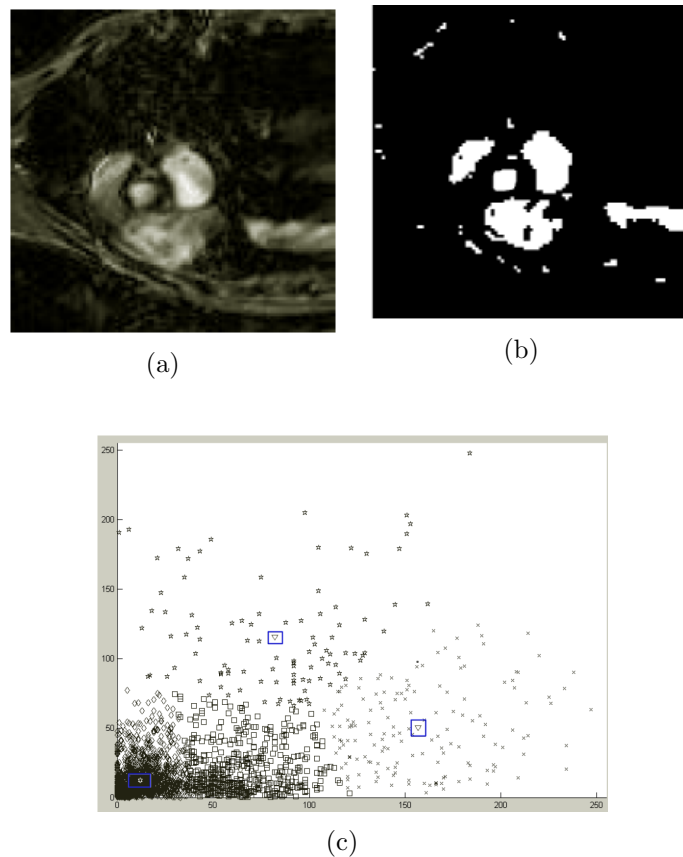


Figure 2.6: Segmentation result using clustering algorithms [23]. (a) Input MR image. (b) Segmented image. (c) Clusters and centers. Points with the same mark belong to the same cluster. Cluster centers are indicated by large boxes.

2.2.1 Deformable Models

Deformable models delineate region boundaries using curves or surfaces represented by explicit or implicit functions. Snake and level set are two widely used deformable models for the segmentation of vasculatures. Active shape is another well-known deformable model. But, it is not used for segmenting vasculatures because their shapes are too complex to be described by active shape model. So, it is ignored in this discussion.

Snake

Snake, also called active contour models, was first proposed by Kass, Witkin, and Terzopoulos [36]. Snake is a contour represented by connected points. It behaves like a rubber band and can be deformed to match any shape under the influence of internal force, image force and external force. These three kinds of forces are defined so that the snake will conform to an object boundary or other features in the image. The internal energy is associated with elasticity and rigidity of the snake. The image energy specifies the image feature, such as edges, used to attract the snake. The external energy is not often used, and it can be spring energy, repulsion and so on. When the sum of these three kinds of energy is minimized, the snake should approach the desired image features.

Snake is a good model which can be used in many applications. Snake will fit the contour of any shape as long as the forces are well designed and balanced. It can connect disjoint edges by finding an optimal compromise between different forces. Moreover, it guarantees a smooth and closed boundary of the desired object. However, it has some intrinsic shortcomings. For instance, it can be very sensitive to initialization and noise, and it cannot fit well to concave features (Figure 2.7) [75].

To overcome these shortcomings, Xu and Prince proposed the gradient vector flow (GVF) method [75]. GVF field is a vector field derived from the diffusion of the gradient vectors of a gray-level or binary edge map computed from the input image. GVF replaces the usual image forces, and it can attract the snake to fit the concave part of the object in the image (Figure 2.7). Although GVF is less sensitive to initialization than traditional snake, it still requires a good initialization. It can also be distracted by noise.

Another variation is the dual snakes [26]. In this case, two snakes are used. One is an interior snake lying within the regions of the desired object. The other is an exterior snake outside the desired regions. The two snakes are coupled using spring energy that causes them to be attracted to each other as well as the boundary of the desired object. Dual snake model incorporates the information from two snakes approaching the desired boundary from both sides. It reduces sensitivity to initialization. It also provides good performance in the case of non-convex shapes.

Yezzi et al. derived a new active contour model for edge detection and segmentation of MRI, CT, and ultrasound medical images [78]. It amounts to curve evolution together with a stopping term. The evolution follows the gradient direction in which the curve shrinks as fast as possible. The active contour will stop at the desired edges by minimizing the geometric energy based on the gradient flow of the active contour (Figure 2.8).

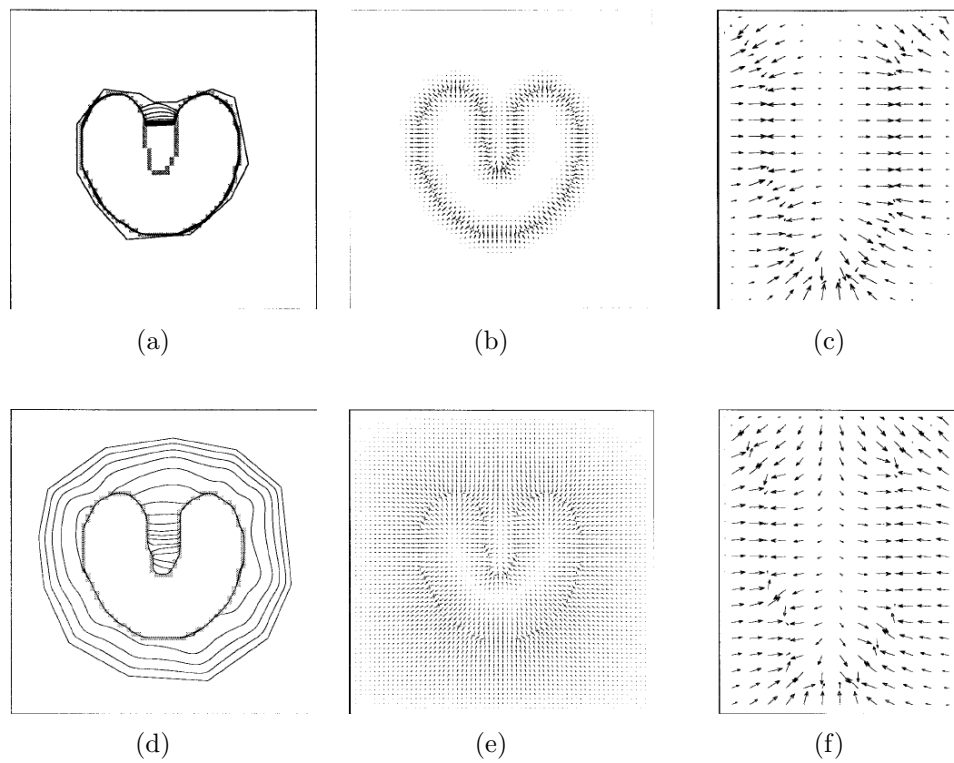


Figure 2.7: Comparison between traditional snake and GVF. (a) Convergence of a traditional snake, (b) traditional potential forces, (c) close-up of the concave part, (d) Convergence of a GVF snake, (e) GVF external forces, and (f) close-up of the concave part of GVF [76].

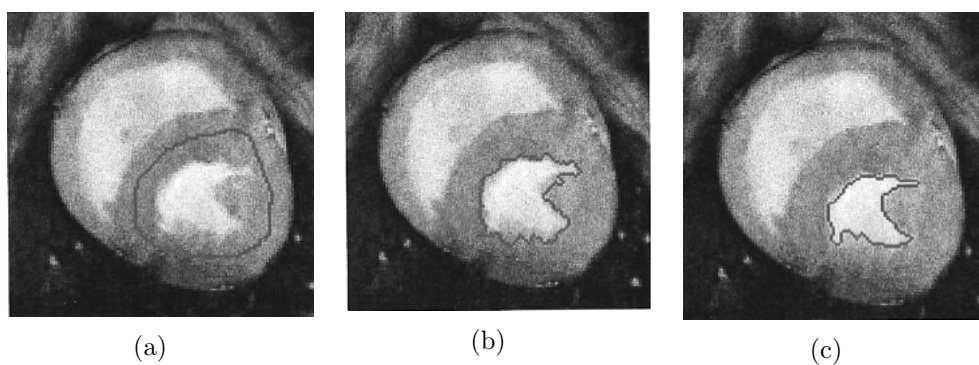


Figure 2.8: Contour extracted from MRI heart image via snake [78]. (a) The initial contour, (b) the intermediate contour during evolution, and (c) the final contour.

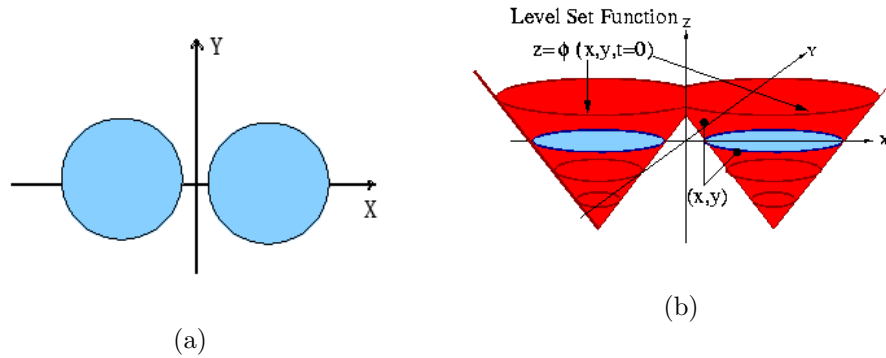


Figure 2.9: (a) 2-D contours. (b) The level set surface (in red). The zero level set (in blue) gives the 2-D contours.

Level Set

Level set was proposed by Osher and Sethian [53]. It represents the interface (2-D contour or 3-D surface) in one higher dimension.

Consider, for example, a 2-D contour Γ (Figure 2.9(a)). A level set function $\phi(x, y, t)$ (the red surface in Figure 2.9(b)) is defined in 3-D. Typically, ϕ is the signed distance function to the contour. It keeps all possible states of Γ . The intersection of $\phi(x, y, t)$ and the x - y plane gives the contour Γ . Therefore, at any time t , Γ can be obtained by solving the equation $\phi(x, y, t) = 0$.

The level set function $\phi(x, y, t)$ moves up and down the ϕ -axis under some predefined forces that give the propagation velocity of Γ . The initial position of Γ is given by the initial contour of $\phi(x, y, t = 0)$. Numerical schemes are applied to approximate the equations of motion to compute $\phi(x, y, t + \Delta t) = 0$ given $\phi(x, y, t) = 0$. The evolution will iterate until the level set function $\phi(x, y, t)$ converges.

Level set is used in many applications [45, 61, 66]. A simple 2-D example is shown in Figure 2.10 [66]. Starting from a small circle within the vessel, the contour expands to fit the boundaries of the blood vessels. The idea of level set can be easily extended to 3-D cases to extract surfaces of the desired objects [39, 44, 51].

The primary advantage of level set method is that the level set function remains a single function even when the zero level set changes topology, breaks, merges, or forms sharp corners when it evolves over time. There-

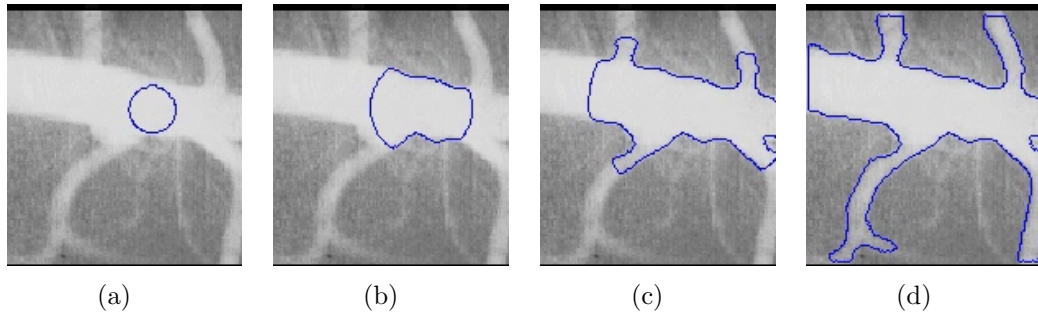


Figure 2.10: The evolution of the zero level set curve [66]. (a) The initial contour, (b, c) intermediate contours during evolution, and (d) the final contour of the blood vessel.

fore, level set is useful for segmenting objects with complex topology such as blood vessels. However, traditional level set method does not contain geometrical constraints. So, the zero level set may leak into some undesired regions.

In general, the ϕ value of every pixel has to be computed at each iteration. Efficient algorithms such as narrow band [1] and fast marching [67] are developed to improve the efficiency of level set method. In narrow band method, the ϕ values are computed for the pixels within a narrow region around the propagating contour only because the pixels far away from the contour do not affect its propagation. Fast marching is applicable when the contour always propagates in the same direction.

2.2.2 Atlas-based Approach

Atlas-based approach is powerful and widely used when a standard template called the atlas is available. It exploits prior anatomical knowledge in segmentation. Usually these algorithms solve the segmentation problem using registration technique to align the atlas and the image.

As shown in Figure 2.11(a), the atlas contains contours of the desired objects. The first step is to place the atlas near to the desired objects by global transformation including scaling, translation and rotation (Figure 2.11(b)). Then, each atlas contour is deformed to fit the boundary of the desired objects. Once the deformation of each contour is completed, the image is segmented into several parts, and each one corresponds to one part

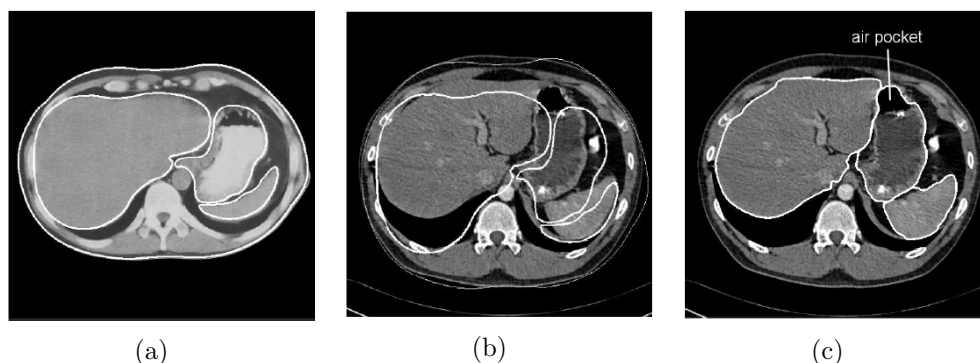


Figure 2.11: Atlas-based segmentation example [17]. (a) Atlas contours (white curves) superimposed on the reference CT image. (b) Atlas registered onto a target image after global transformation. (c) Final segmentation result.

in the atlas.

Atlas-based algorithms do not suffer from over-segmentation because of the one-to-one correspondence between the atlas regions and the segmented regions. Due to the strong shape constraints from the atlas, they have less leakage problems than deformable model without shape constraints. Furthermore, it can provide a good initialization for snake and level set. However, building an appropriate atlas can be quite difficult. If atlas is constructed from a single image, it may not be representative of the desired object. On the other hands, constructing an atlas from a set of images requires more work.

2.3 Comparison of Segmentation Methods

Based on the discussion given in Sections 2.1 and 2.2, the strengths and weakness of the various segmentation methods are summarized as follows (Table 2.1). Atlas-based approach is the least sensitive to noise. The other algorithms are all sensitive to noise with thresholding being the most sensitive.

Thresholding, classification and atlas-based approach do not need any initialization except for setting some parameters and training sets. Level set is less sensitive to initialization than snake. Snake, region growing and watershed are very sensitive to initialization.

Table 2.1: Comparisons of segmentation methods

Algorithms	Sensitivity to noise	Sensitivity to initialization	Severity of over-segmentation	Complexity of image solvable
Thresholding	Very high	No	Very high	Very low
Region growing	High	High	High	Low
Watershed	High	High	High	Low
Classification	Moderate	No	Moderate	Moderate
Clustering	High	Moderate	High	Moderate
Snake	High	High	No	High
Level set	High	Low	Low	High
Atlas-based	Low	No	No	High

Snake and atlas-based approach will not over-segment the input images. Level set has low probability of over-segmentation. Classification, clustering, region growing, watershed and thresholding suffer from severe over-segmentation.

Atlas-based approach, snake and level set can segment very complex images. Classification, clustering, region growing, watershed and thresholding only can handle simple images by themselves.

2.4 Vascular Structure Segmentation Algorithms

The following is a discussion of specific algorithms for the segmentation of vascular structures in medical images. These algorithms can be divided into seven categories, namely centerline detection, region growing, matched filter, classification, deformable model-based, geometric parametric model-based and stochastic approach.

2.4.1 Centerline Detection

The main idea of the centerline detection approach is to find the centerlines of the entire vascular structure. One type of centerline detection approach is the ridge-based algorithm [8, 21]. It treats a gray-scale image as a 3-D elevation map where intensity ridges approximate the skeleton of the vasculature. Ridge points, which are local peaks in the direction of maximal

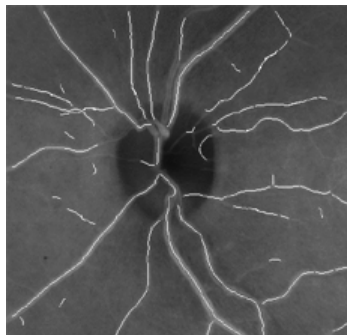


Figure 2.12: Tracked centerlines of retinal blood vessels [8].

surface gradient, are first detected. Then, the whole vascular structure is extracted by connecting neighboring ridge points.

Chandrinos's algorithm [8] detects ridge points based on the gradient of Gaussian smoothed image. Then, the centerlines are obtained by connecting nearest ridge points (Figure 2.12). The algorithm of Florin et al. [21] determines a ridge point by examining the intensity value, peak shape and distance to the heart wall. Ridge points are then linked by a minimum spanning tree algorithm.

Through centerline extraction, topological information of the vascular structure is obtained. It does not require special initialization. But, due to sensitivity to noise, it is difficult for centerline detection methods to extract all the small vessels.

2.4.2 Region Growing

As discussed in Section 2.1.2, region growing approach is designed to search for similar pixels (voxels) according to some predefined criteria of similarity. Region growing is very sensitive to the selection of seed points and susceptible to noise corruption. Sometimes, it is combined with thresholding technique to restrict the candidate seed points [2, 30, 65].

An ordered region growing algorithm [79] has been developed to produce an acyclic graph representation of the MRA image (Figure 2.13). It requires users to specify seed points. Directed edges are established from each seed point to its neighbor points. The directed graph describes the connectivities between all voxels in the image. So based on it, vessel paths and branching patterns of vascular tree can be tracked starting from the points at the ends of vessel branches.

Traditional region growing segmentation frequently fails due to its sensitivity to noise in the images taken with low-dose contrast agent injected. Tschirren uses a multi-seeded region growing method based on fuzzy connectivity [73]. Fuzzy connectivity expresses the similarity of two adjacent voxels as a fuzzy membership value between 0 and 1 according to the difference between their intensities. If two voxels are not directly adjacent, their similarity is determined by looking at all possible chains that connect these two voxels. A chain is a sequence of adjacent voxels. The strength of a chain is defined by the lowest similarity of the adjacent voxels along the chain. The strength of the strongest chain is chosen to represent the similarity of two indirectly adjacent voxels. Tschirren's algorithm sets more than one seed point, and grows two regions of foreground and background simultaneously, letting them compete for voxels according to fuzzy connectivity (Figure 2.14).

2.4.3 Matched Filter

Matched filter extracts vascular structure by convolving the image with predefined filters that characterize the features of vascular structures [9, 10, 11, 31, 47]. Various filters have been applied. In [9], a Gaussian-shaped curve is used to approximate the profile of the cross section of a blood vessel. Based on it, a set of filters are constructed to search for vessel along all possible directions. A half-elliptic cylinder-shaped filter (Figure 2.15(b)) is applied in [22]. Matched filters of various orientations and sizes are convolved with the digital subtraction angiogram (DSA). At each position, the filter with the highest match value is returned as the result (Figure 2.15(c)). In [64], a multi-scale 3-D line enhancement filter based on Hessian matrix is used to discriminate line structure of vessels from background. Matched filter based on Gabor Filter [14] is used to detect X-junctions and T-junctions [10, 11].

Matched filter algorithm is immune to the usually high noise level in angiograms. It returns a high value only when both intensity and spatial properties of the structures match the filter well. The size of the filter affects the computation complexity of the algorithm.

2.4.4 Deformable Model-based Approaches

Deformable model-based approach can deform the model to any shape depending on predefined forces. Therefore, it is useful for vascular structure segmentation because vasculature often has complex 3-D structure. There are two kinds of deformable models that are widely used in the extraction of vascular structures: snake [41, 50, 63] and level set [44, 51, 77].

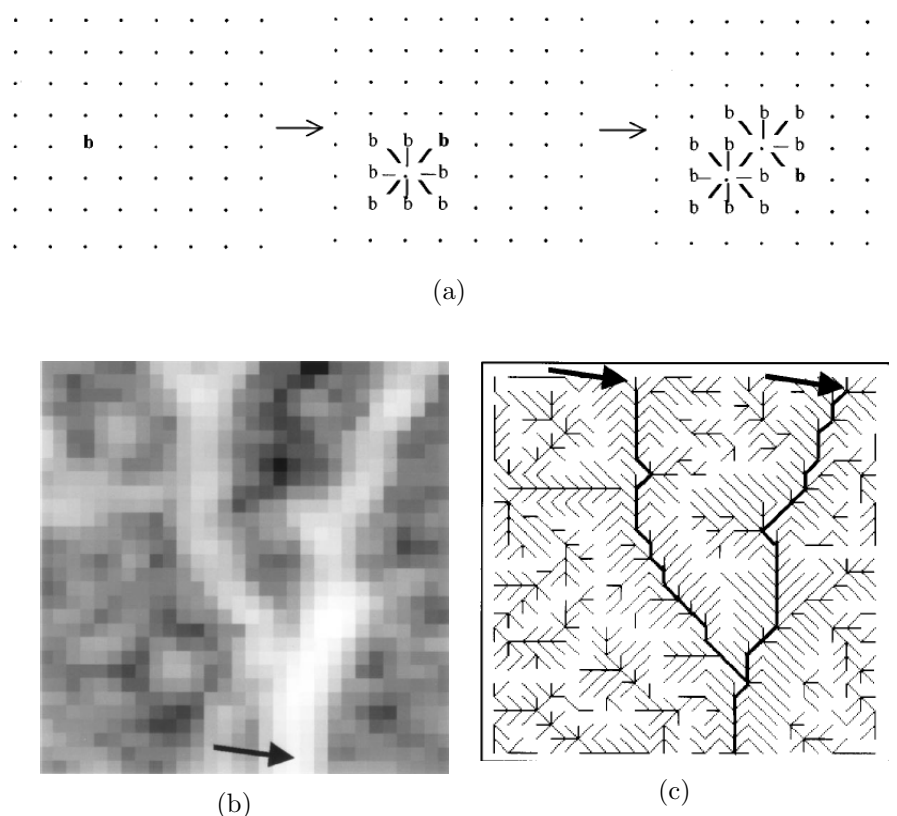


Figure 2.13: Acyclic graph representation of input image [79]. (a) Adjacent points are added to a seed point to form the connectivity graph. (b) An input image. (c) The acyclic graph representation. Lines represent the connectivity between pixels, and arrows indicate the starting points for tracking vessel branches.

In [50], a cubic B-spline snake is used to extract the catheter from biplane angiograms. Initialization is provided by the user. In [63], an adaptive snake is evolved using a stochastic relaxation technique called simulated annealing [37] to find a global energy minimum in noisy MR images (Figure 2.16).

Level set is another deformable model-based algorithm [44, 51, 77]. As discussed in Section 2.2.1, level set method often has leakage problems. To overcome it, a level set model with a soft shape prior, called shape driven flow, is applied to segment 2-D/3-D vessels [51] (Figure 2.17). Moreover, by including both intensity and shape information, this algorithm can overcome leakages near the areas where image information is ambiguous.



Figure 2.14: Segmentation result of intrathoracic airway trees from low-dose CT scan.

2.4.5 Geometric Parametric Model-based Approach

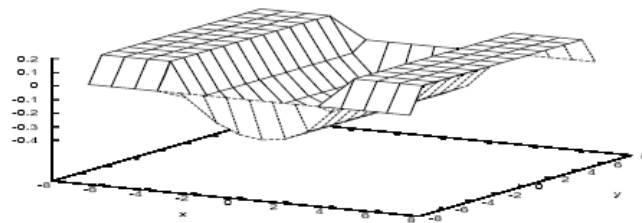
Vasculatures are tube-like objects. Consequently, the cross-section of each vessel can be approximated by an ellipse. Geometric parametric model-based approach aligns a parametric elliptic model with vessel cross-section in every 2-D slice of a 3-D volumetric image to obtain a best fit [6, 20, 56]. Each branch of the blood vessel is represented by a medial axis curve together with an elliptical surface that represents the vessel surface (Figure 2.18(a)). The location of the axis and the parameters of the ellipse are determined to match the model with the input image.

In [20], a two-stage deformation is applied to match the image. The first stage called axis deformation determines the position of each elliptic model for each vessel according to the medial axis (Figure 2.18(c)). The second stage performs a surface deformation to determine the parameters of the elliptic model, such as semidiameter and orientation (Figure 2.18(d, e)).

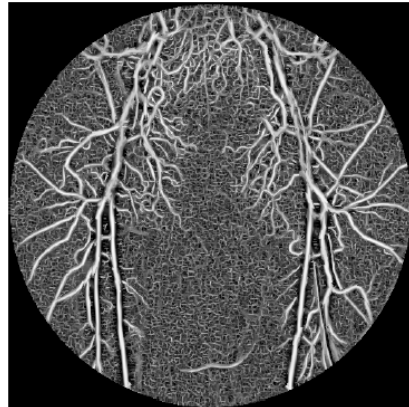
Geometric parametric model-based approach is applicable to the segmentation of healthy vasculature. It does not have leakage problem because it always preserve the shape of each cross-section of the vasculature. However, it has some intrinsic problems. Cross-section of vasculature might not have an elliptic shape when it is unhealthy. Under such circumstances, geometric parametric model may not be appropriate.



(a)



(b)



(c)

Figure 2.15: Matched filter used by Franz [22]. (a) Input DSA, (b) matched vessel filter, and (c) matched filter result.

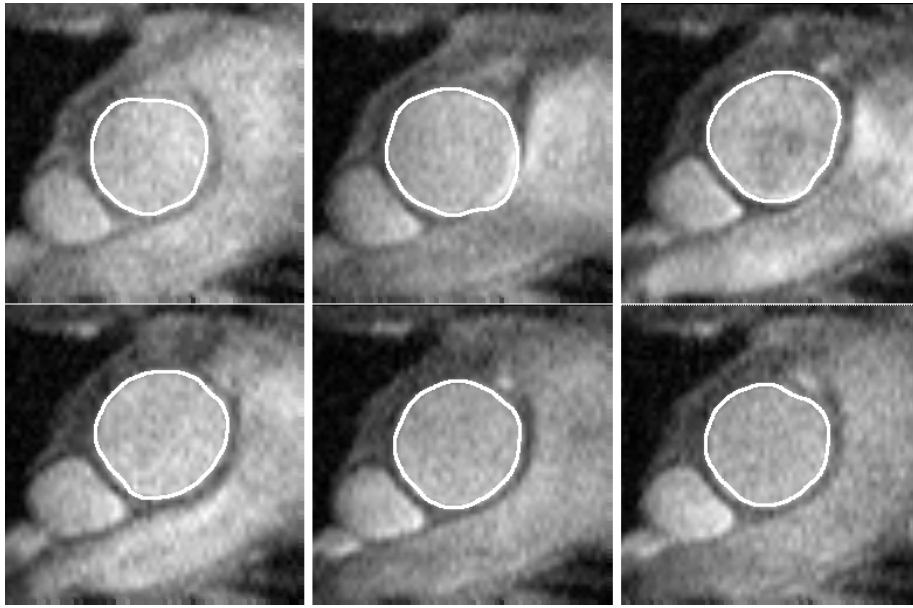


Figure 2.16: Segmentation results of the ascending aorta from consecutive frames using adaptive snake [63]. The result of each frame is used as the initialization for segmentation for next frame.

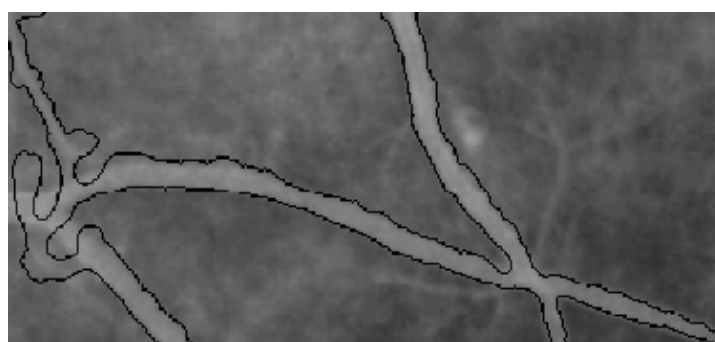
2.4.6 Classification

The basic idea and pros and cons of classification-based segmentation have been discussed in Section 2.1.4. Nekovei and Sun [52] developed a neural-network classifier for extracting blood vessels in angiograms. The multilayer feed-forward network learns to classify pixels according to their intensities using back-propagation learning algorithm. Soare et al. [70] developed a method for automated segmentation of the vasculature in retinal images using a Bayesian classifier. Features are extracted through 2-D Morlet wavelet transform in the green channel of the input images.

Hassouna and Farag [29] used classification algorithm to classify voxels into two classes, namely background and vessels, according to the intensity distribution of the images is characterized. The background intensities are modeled by a finite mixture of a Rayleigh [55] and two normal distributions, while blood vessels are modeled by normal distribution. Whether a voxel belongs to the vessel class is determined according to maximum a posteriori (MAP) classification.



(a)



(b)



(c)



(d)



(e)

Figure 2.17: 2-D and 3-D segmentation results using shape driven flow [51]. (a) 2-D result without shape prior level set. Contour leaks into several non-vessel regions. (b) 2-D result with shape prior has a less severe leakage problem. (c) 3-D results without shape prior. The leakage connects with the vessel to the background. (d) 3-D result with shape prior has no leakage problem. (e) Final segmentation result from a different viewpoint.

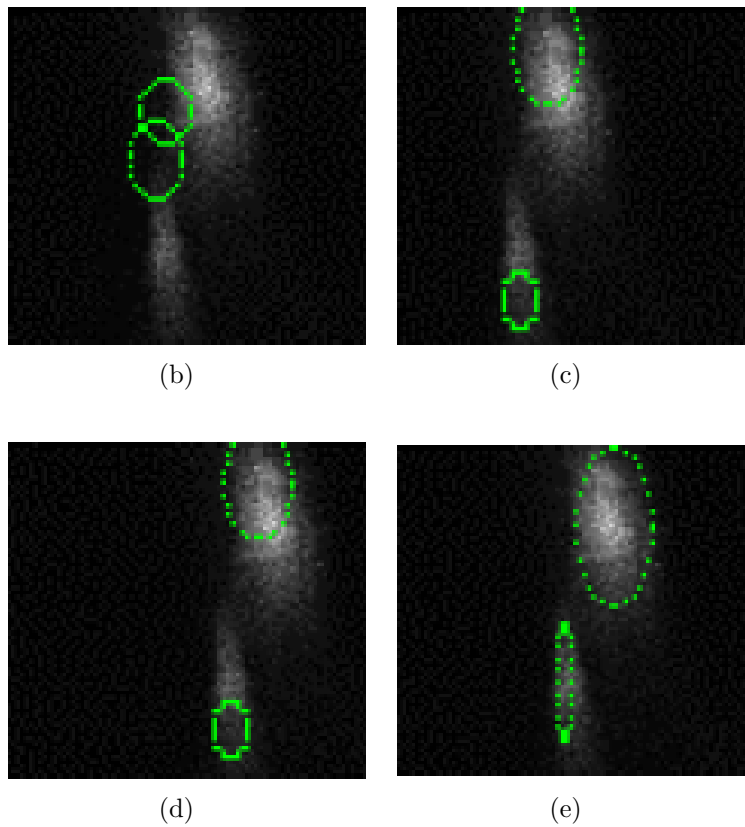
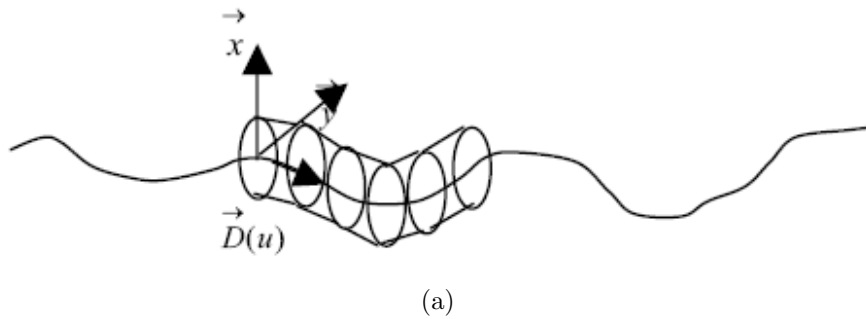


Figure 2.18: Deformation procedure of a pair of vessel cross-sections [20]. (a) Medial axis of a branch and its elliptic circumference. (b) The initial contours of vessel cross-sections. (c) Contours after one iteration of axis deformation. (c) Contours after one iteration of surface deformation. (d) Final contours after axis and surface deformation.

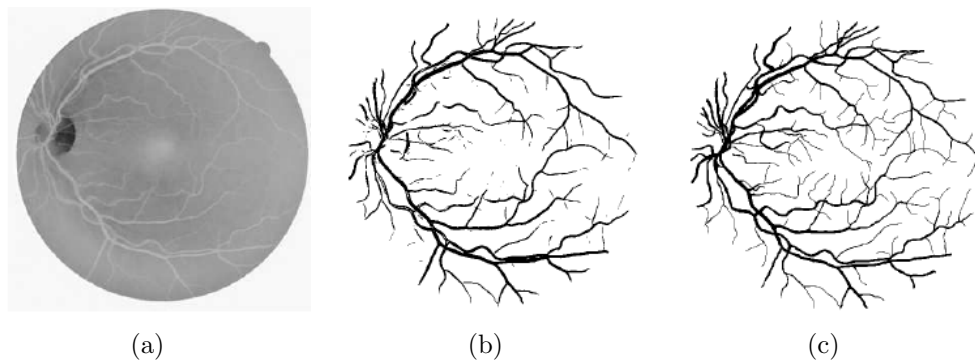


Figure 2.19: Segmentation result of a retinal image using classification algorithm [70]. (a) The inverted green channel of retinal image. (b) Segmentation result produced by the algorithm. (c) Manual segmentation result.

2.4.7 Stochastic Approach

Stochastic approach segments images of vascular structures using stochastic processes [42]. The vascular structure is represented as a set of segments. Each segment is modeled by a set of random variances that describe its position, orientation, length, etc. Geometric constraints, such as continuity of segment network and local curvature, are incorporated as the probability of the connection between two segments.

The algorithm iteratively seeks the configuration of random variables that maximizes the probability of constructing the entire vessel tree (Figure 2.20(b)). It starts from an initial random configuration. It updates the configuration using algorithms such as simulated annealing until an optimal solution is found.

Stochastic approach integrates geometric constraints into the segmentation process. It can obtain the topology of vascular structure. It is immune to noise and does not suffer from over-segmentation. On the other hand, the complexity of stochastic algorithm is usually very high.

2.4.8 Summary

Based on the discussion in the previous sections, comparisons between the algorithms are summarized as follows (Table 2.2). All the algorithms are sensitive to noise except for geometric parametric model and stochastic approach that incorporates geometric constraints.

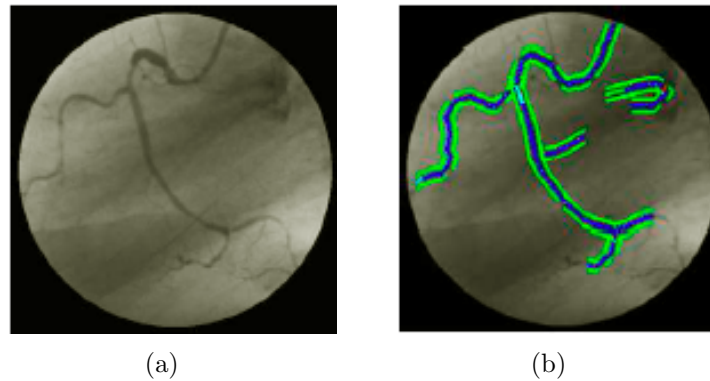


Figure 2.20: Coronary tree extraction in [42]. (a) A 2D x-ray angiographic image. (b) Coronary extraction result.

Centerline detection, matched filter, classification and geometric parametric approach do not require any initialization. Level set and stochastic approach are less sensitive to initialization than region growing and snake.

Snake and geometric parametric approach do not suffer from over-segmentation. Level set, stochastic approach, and centerline detection has a low probability of over-segmenting an input image. Matched filter, classification, and region growing can result in over-segmentation.

All the algorithms except snake can be applied to segment and obtain complex vessel tree of vasculature from input images. Snake is used for segmenting the simple contours of cross-section of vasculature from each slice of CT/MR images.

Table 2.2: Comparisons of vascular segmentation algorithms.

Algorithms	Sensitivity to noise	Sensitivity to initialization	Severity of over-segmentation	Vessel tree
Centerline detection	High	No	Low	Yes
Region growing	High	High	High	Possible
Matched filters	Moderate	No	Moderate	Possible
Classification	Moderate	No	Moderate	Possible
Snake	High	High	No	No
Level set	High	Low	Low	Yes
Geometric parametric model	Low	No	No	Possible
Stochastic Approach	Low	Low	Low	Yes

Chapter 3

Possible Research Topics

Based on the literature review in Chapter 2, some possible research topics about 3-D vascular structure segmentation from temporal sequences and segmentation and annotation of multiple parts of 3-D cardiac blood vessels are presented as below.

3.1 Segmentation of Blood Vessels from Temporal Sequence of Angiograms

Blood vessels change intensity, location and shape over time, and they do not always appear clearly visible in the temporal sequence of angiograms due to the pumping of the heart and the flowing of contrast agent along with the blood (Figure 3.1). And in angiograms, the blood vessel boundaries sometimes become blur. Therefore, a single 2-D image is not enough to segment angiograms correctly. But existing algorithms discussed in Section 2.4 are mainly designed for single 2-D, and may not work well with unclear boundaries.

To achieve a complete and correct segmentation of blood vessels in angiograms, a temporal sequence is required. The primary problem lies in how to finding the appropriate relationship between different slices taken at different time. And the relationship is useful to track the positions and shapes of blood vessels in each frame of the temporal sequence.

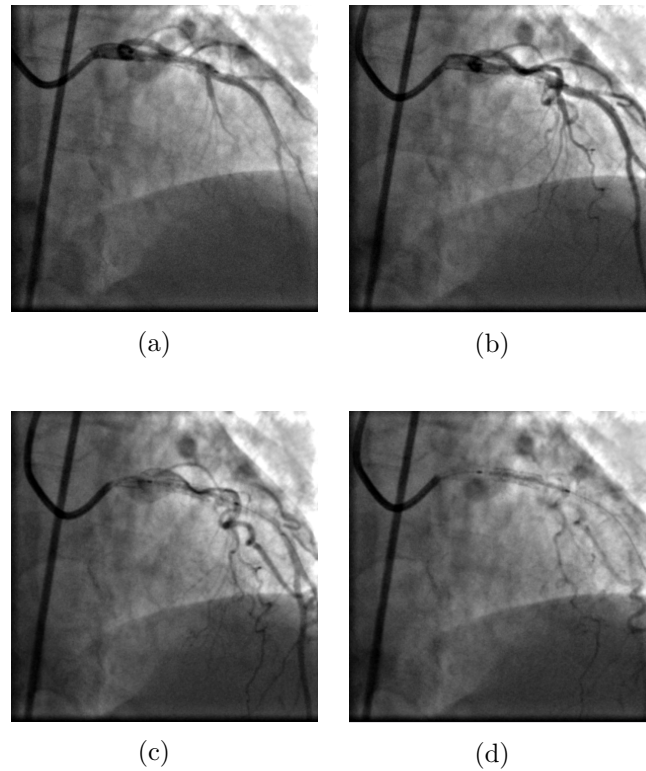


Figure 3.1: Example of 2-D temporal sequence of cardiac angiograms. Blood vessels change position, shape and intensity over time.

3.2 Segmentation and Annotation of Multiple Parts of 3-D Cardiac Vasculature

Some of the algorithms discussed in Section 2.4 can be used to perform 3-D segmentation of cardiac vasculature. They will produce a 3-D structure of cardiac vasculature as a whole. For practical use, it is necessary to separate the 3-D structure into various anatomical parts such as ascending aorta, descending aorta, aortic arch and veins.

To segment and annotate multiple parts of 3-D cardiac vasculature, a 3-D atlas that describes the various parts of the cardiac structure is required. There are some main difficulties in separating the various parts. The 3-D structure of the cardiac vasculature is very complex. Main arteries are close to each other (Figure 3.2). The boundaries between them are, in many

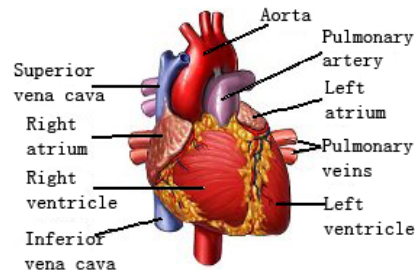


Figure 3.2: 3-D structure of the main cardiac vasculature.

cases, ambiguous in the CT/MR images. And relative positions and shapes of the cross-sections are not the same in different slices. Therefore, it is difficult to construct an effective 3-D atlas to describe the entire structure with separate parts. In addition, the atlas is also hard to be used to perform the segmentation.

Chapter 4

Preliminary Work

4.1 Characteristics of Input Images

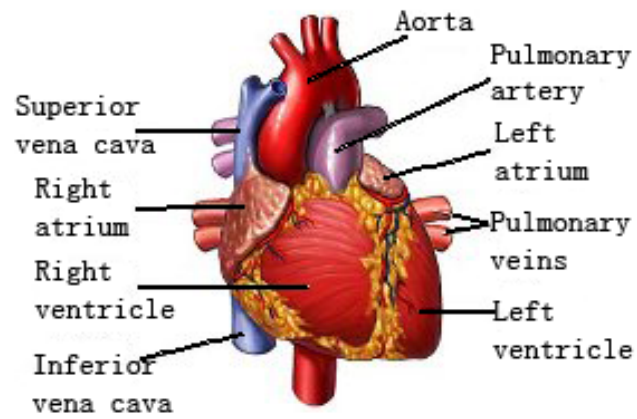
The input images are a 3-D volume of thoracic CT slices of cardiac blood vessel (Figure 4.1). x - and y -axis are horizontal and vertical axes in each slice. z -axis is the slice number. The resolutions of x - and y -axes are usually the same. And the resolution of z -axis is usually different from those of the x - and y -axes.

As seen in Figure 4.1, the blood vessels appear brighter than the background and other tissues. The edges between vessels and the background are distinctive, but the edges between the blood vessels and other tissues are sometimes not distinctive.

4.2 Problem Description

The task is to segment the cardiac vasculature of a 3-D volumetric image of thoracic CT (Figure 4.1). The main vessels, such as ascending aorta, descending aorta, aortic arch, veins, and pulmonary aorta, are required to be segmented as automatically as possible, and then the 3-D structure of vessels should be visualized.

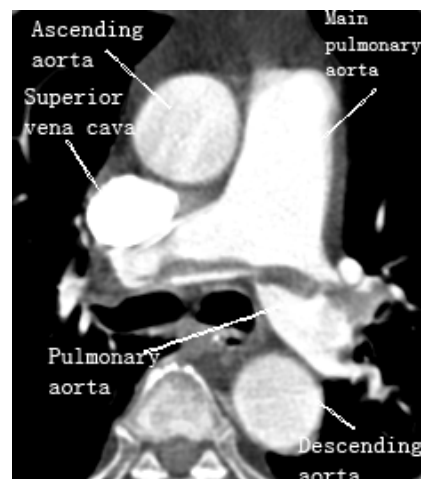
The problem with automatic segmentation of 3-D blood vessels can be considered as finding a appropriate deformation to an initial surface so that it can separate the blood vessels from other parts of the images.



(a)



(b)



(c)

Figure 4.1: A 3-D model of heart and two sample CT slices of the heart with the main vessels highlighted.

4.3 Algorithm

The algorithm can be divided into three main stages: preprocessing, level set evolution, and visualization.

4.3.1 Preprocessing

There are two steps in preprocessing: linear interpolation and filtering.

Linear Interpolation

As discussed in Section 4.1, the resolution of z -axis is usually different from those of the x - and y - axes. Therefore linear interpolation is performed along z - axis to normalize the resolutions. Then, each pixel in 2-D slices is represented as a cubic voxel in a 3-D coordinate system.

Filtering

As discussed in Section 2.2.1, the level set method is often confused by the ambiguous boundaries between vessels. As seen in Figure 4.2(a), the gray regions separate vessel A , B and the background. In some regions, the intensity gradients of voxels on the boundaries between vessels and gray regions are more or less the same or even less than those of the voxels on the boundaries between gray regions and background. So it is easy to confuse the level set method that is mainly based on intensity gradients.

Therefore the main objective of this step is to remove these gray regions in CT slices.

To achieve this objective, a filtering process is applied as follows:

$$\begin{aligned}
 I_T(v) &= \begin{cases} I(v) & \text{if } g(I(v)) > T \\ 0 & \text{if } g(I(v)) \leq T \end{cases} \\
 g(I(v)) &= \frac{1}{n} \sum_{v' \in N(v)} I(v')
 \end{aligned} \tag{4.1}$$

where n denotes the number of neighboring voxels, $N(v)$ represents the set of neighboring voxels, and T is a threshold.

Before filtering, the threshold value T is determined as follows. First, extract gray and white regions from a set of slices to construct an intensity histogram (Figure 4.2(c)). Next, k -means clustering ($k = 2$) is applied to cluster the sample data into two clusters according to intensities. The initial cluster centers are set to 0 and 255 respectively. After k -means clustering the average between the two cluster centers is computed and used as the threshold T .

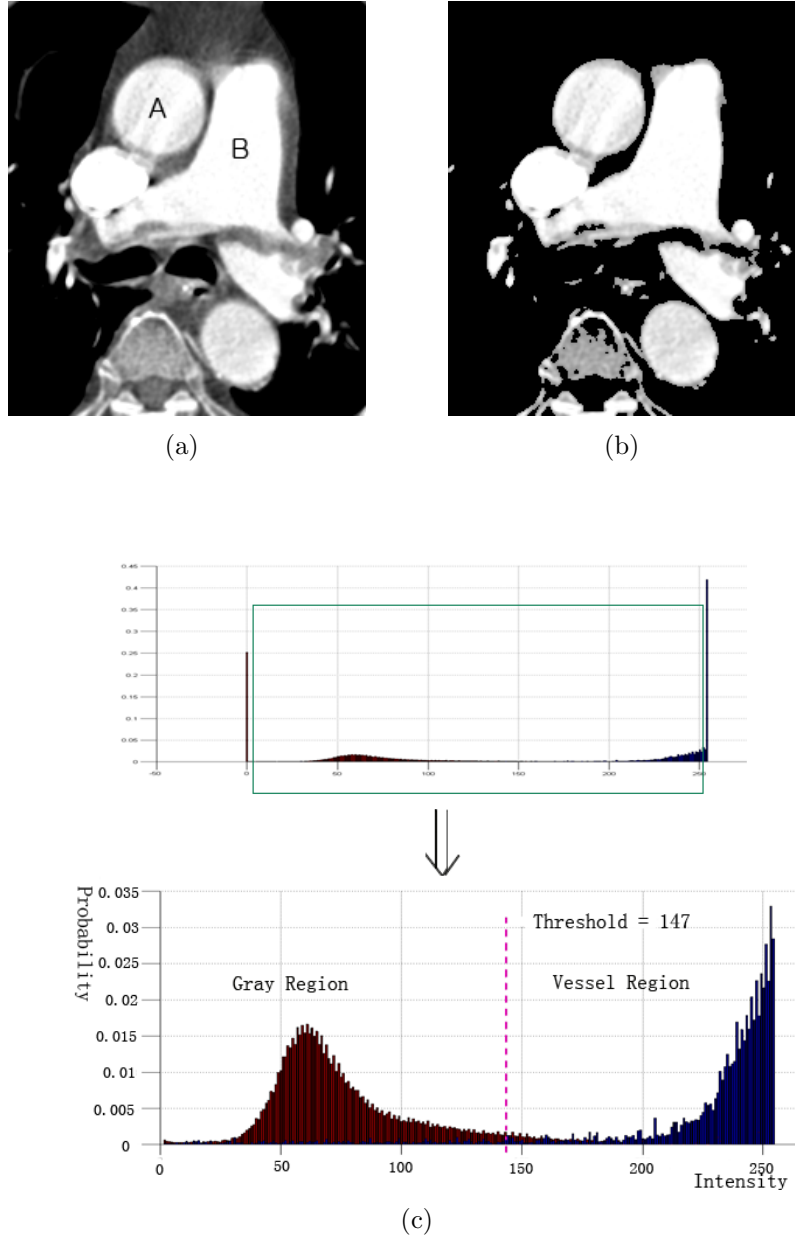


Figure 4.2: (a) Blood vessels A and B are separated by a gray region, (b) the image after filtering, (c) intensity histogram of training data.

4.3.2 Level Set Evolution

Level set algorithm is used to evolve an initial surface. Three aspects of this method are discussed, namely initialization, evolution equations and stopping criteria.

Initialization

Region growing technique is run on the filtered image to search for a white connected component starting from any white voxels. Next, a small sphere located inside the white connected component is generated as the initial surface of level set algorithm. The size of the sphere does not matter.

Level Set Evolution Equations

The level set algorithm is governed by the following equations [45]:

$$\frac{\partial \phi}{\partial t} = c(v)(\epsilon\kappa + V_0)|\nabla\phi| + \beta\nabla P \cdot \nabla\phi \quad (4.2)$$

$$P(v) = |\nabla(G_\sigma * I_T(v))| \quad (4.3)$$

$$c(v) = \frac{1}{1 + P(v)} \quad (4.4)$$

where ϵ , V_0 , β are constants. $I_T(v)$ denotes the filtered 3-D image and it is Gaussian smoothed to obtain $P(v)$ to reduce noise. $\nabla P \cdot \nabla\phi$ denotes the projection of a force vector on the surface normal. It attracts the zero level set to the edges in the image. It can also help to smooth the surface. $c(v)$ is a stopping term. It becomes smaller when the level set surface approaches the edges in the image.

Stopping criteria

Let R and R' denote the point sets on the zero level sets of two consecutive iterations respectively. Define the difference between these two sets as:

$$d(R, R') = \frac{1}{|R|} \sum_{v \in R} \min_{v' \in R'} \|v - v'\|. \quad (4.5)$$

When $d(R, R')$ is smaller than a predefined constant ϵ' , the zero level set does not change significantly between the two iterations. Therefore, the algorithm can stop.

4.3.3 Visualization

The segmentation results obtained by level set algorithm is represented as a signed distance function. Voxels within blood vessels have negative distance to the level set surface, and background voxels have positive distance. However, most of the 3-D model viewers only accept vertex-and-mesh model as input. Therefore, marching cubes algorithm [43] is utilized to convert the result to 3-D model represented by vertices and triangle meshes.

4.4 Experiments

Experiment was conducted on a set of thoracic CT slices to test the algorithm described in Section 4.3. Qualitative and quantitative evaluations of the performance of the segmentation algorithm were carried out.

The test images are 87 thoracic CT slices of a patient. The thickness between two consecutive slices is 1 mm, and the pixel spacing in every slice is 0.66 mm.

In preprocessing, resolution of the 3-D volumetric image was changed to $0.66 \text{ mm} \times 0.66 \text{ mm} \times 0.66 \text{ mm}$ through interpolation. Then, gray and white regions were extracted manually from 30 slices. Next, k -means clustering with $k = 2$ was applied to obtain the threshold $T = 147$. All the slices were filtered according to Equation 4.1 with $T = 147$.

In the next stage, the level set algorithms implemented by Mitchell [48] was used to segment the filtered images. The initial surface of level set was obtained by region growing as discussed in Section 4.3.2. The parameters of level set evolution (Equation 4.2) were set as follows: $\epsilon = 0.025$, $V_0 = 0.5$, $\beta = 1$ and $\sigma = 3.25$.

Finally, the implicit surface produced by level set was transformed to mesh model using Public Domain Polygonizer [5] that was an implementation of marching cubes algorithm.

3-D mesh mode of segmentation result is visualized by quick3D viewer (Figure 4.3). Main vessels, such as ascending aorta, descending aorta, pulmonary aorta and superior vena cava, are extracted from the volumetric image.

Both qualitative and quantitative evaluation were conducted to evaluate the performance of the algorithm.

Qualitative Evaluation

The effect of filtering in the pre-processing stage was compared. Level set algorithm was run on the images without filtering and with filtering separately. Without filtering, the level set surface could not stop at the boundaries of vessels (Figure 4.4(a)), because the intensity gradients of the

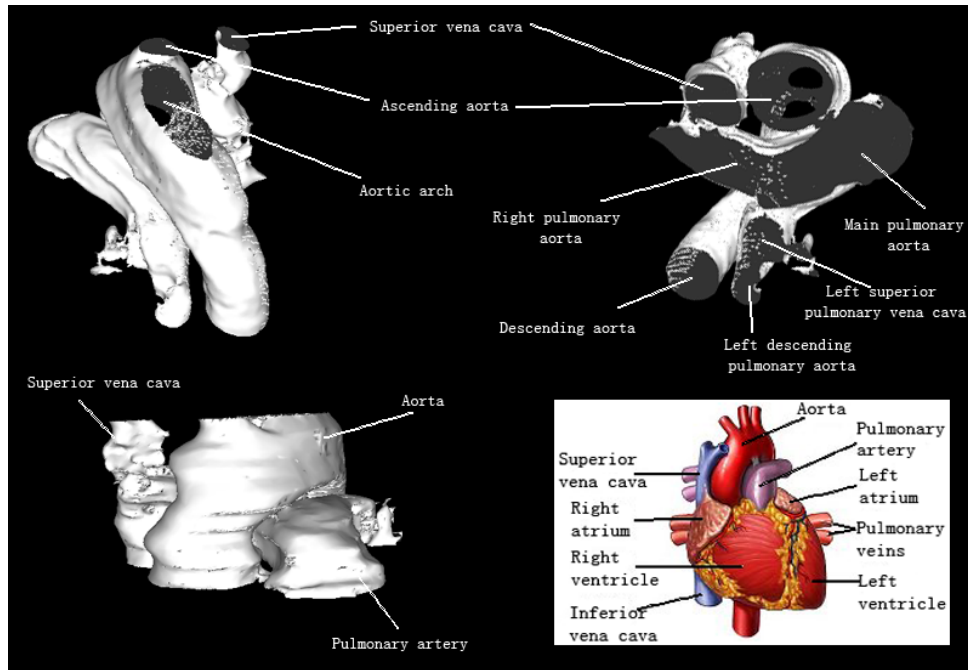


Figure 4.3: Final 3-D segmentation result from different views.

voxels on the boundaries between the blood vessels and the gray regions were small. The surface leaks into the gray regions (Figure 4.4(a)). After filtering, most of the gray regions were removed. The intensity gradients of the voxels on the boundaries between the blood vessels and black regions are large enough to stop the evolution of the level set surface at the vessel boundaries (Figure 4.4(b)).

In some slices, neighboring blood vessels are incorrectly merged (Figure 4.5). This is mostly likely because the regions between them are similar to the blood vessels in intensity, and the level set surfaces leak out and merge into each other. In this algorithm, only the intensity and the gradient of the intensity were used to constrain surface evolution. Geometric and topological information could be used to prevent such merger.

Quantitative Evaluation

The error of the segmentation results was computed by measuring the differences between the results and ground truth. First, contours were extracted manually from 18 test slices, and they were taken as the ground truth. Let $G = \{p_i\}$ denote the set of points on the contours provided by the

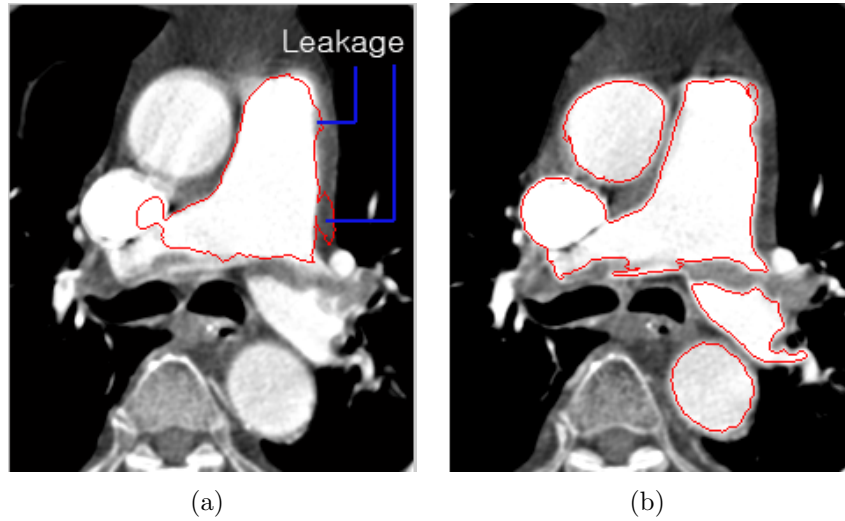


Figure 4.4: Effect of filtering. (a) Intermediate segmentation result without filtering. The level set surface leaks into gray regions. (b) Segmentation result with filtering. Red lines denote the contours obtained by the algorithm.

ground truth, and $R = \{q_j\}$ denote the set of points on the contours in the segmented results. The distance function (Equation 4.5) was used as the error measure. If the average distance between the result and corresponding ground truth is small, it means the contour obtained by the algorithm is close to the ground truth. That is to say the segmentation algorithm performs well.

Figure 4.6 shows the errors of the 18 slices. Compared with the two consecutive slices, the great difference highlighted probably lead to the poor segmentation result, because the large intensity difference in z -axis enlarges the gradient that makes level set surface stop at the wrong place. The segmentation result on the right is much better with correct contours at most of the actual boundaries. In a word, the results show that algorithm is quite stable, and it produce to provide acceptable segmentation of cardiac blood vessels most of the time expect for some special cases discussed above.

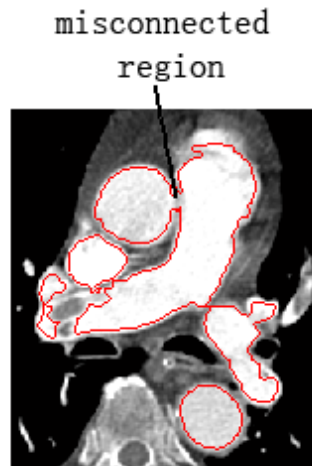


Figure 4.5: Results with merged regions.

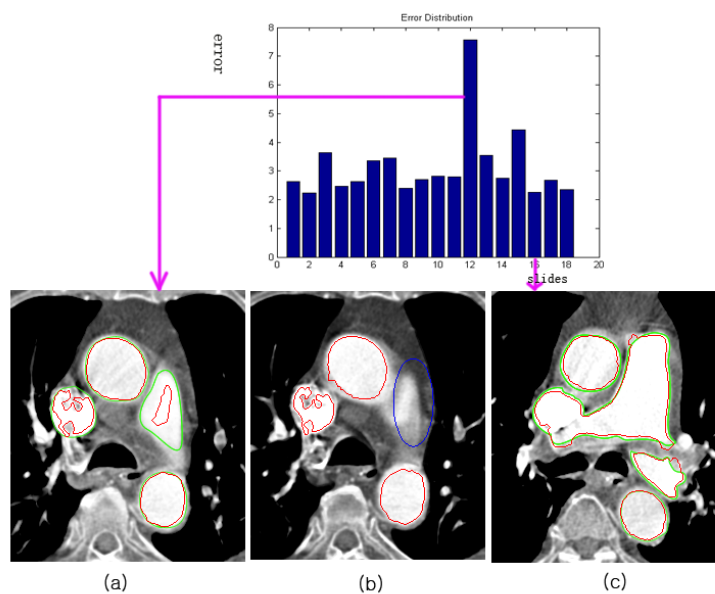


Figure 4.6: Segmentation errors of some CT slices. (a) The result with largest error. (b) The previous slice of (a). The great difference between (a) and (b) is highlighted in blue circle. (c) The result with smallest error. Red lines represent the segmented result of program, and green lines describe the ground truth.

Chapter 5

Conclusion

A thorough literature review of existing segmentation algorithms for medical images, especially vascular structures, is presented in this paper. General segmentation algorithms are categorized into five classes, namely thresholding, region growing, watershed, classification and clustering. General segmentation algorithms are simple and easy to use. However, they cannot handle complex medical images.

There are two kinds of model-based segmentation algorithms, namely deformable model-based approach and atlas-based approach. Both of them can handle more complex images than do the general algorithms. Snake and level set are two widely used deformable model-based algorithms.

Specific algorithms for the segmentation of vascular structures are categorized into seven categories, namely centerline detection, region growing, matched filter, classification, deformable model-based, geometric parametric model-based and stochastic approach.

Based on the literature reviews, two possible research topics are proposed. One is segmentation of blood vessels from temporal sequence of angiograms, and the other is segmentation and annotation of multiple parts of 3-D cardiac vasculature.

Preliminary work is performed on segmenting 3-D structure of main cardiac blood vessels from thoracic CT images. Level set method was applied to segment the 3-D volumetric data. In segmentation results, correct contours of main cardiac blood vessels are obtained. By comparing the segmentation results and ground truth of several slices, it shows that the algorithm could provide acceptable segmentation results most of time.

Bibliography

- [1] D. Adalsteinsson and J.A. Sethian. A fast level set method for propagating interfaces. *Journal of Computational Physics*, 118:269–277, 1995.
- [2] D. Aykac, E.A. Hoffman, G. McLennan, and J.M. Reinhardt. Segmentation and analysis of the human airway tree from three-dimensional X-ray CT images. *IEEE Transactions on Medical Imaging*, 22:940–950, 2003.
- [3] X. Bao, S. Xiao, and Z. Xu. Three-dimensional segmentation of CT images using neural network. In *Proceeding of International Conference of the IEEE*, volume 2, pages 605–608, 1998.
- [4] J.C. Bezdek, L.O. Hall, and L.P. Clarke. Review of MR image segmentation techniques using pattern recognition. *Medical Physics*, 20(4):1033–1048, 1993.
- [5] J. Bloomenthal. *Public Domain Polygonizer*
<http://www.unchainedgeometry.com/jbloom/papers.html>.
- [6] A. Bors and I. Pitas. Object segmentation and modeling in volumetric images. In *Proceeding of Workshop on Non-Linear Model Based Image Analysis*, pages 295–300, 1998.
- [7] K. R. Castleman. *Digital Image Processing*. Upper Saddle River: Prentice Hall, 1996.
- [8] K. Chandrinou, M. Pulu, R. Fisher, and P. Trahanias. Image processing techniques for the quantification of atherosclerotic changes. In *Proceeding of Mediterranean Conference on Medical and Biological Engineering and Computing*, 1998.

- [9] S. Chaudhuri, S. Chatterjee, N. Katz, M. Nelson, and M. Goldbaum. Detection of blood vessels in retinal images using two-dimensional matched filters. *IEEE Transactions on Medical Imaging*, 8(3):263–269, 1989.
- [10] J. Chen, Y. Sato, and S. Tamura. Orientation space filtering for multiple orientation line segmentation. In *Proceeding of the IEEE Computer Society Conference on Computer Vision and Pattern Recognition*, pages 311–317, 1998.
- [11] J. Chen, Y. Sato, and S. Tamura. Orientation space filtering for multiple orientation line segmentation. *IEEE Transactions on Pattern Analysis and Machine Intelligence*, 22:417–429, 2000.
- [12] C. K. Chow and T. Kaneko. Automatic boundary detection of the left ventricle from cineangiograms. *Computers and biomedical research*, 5:388–410, 1972.
- [13] K.S. Chuang, H.L. Tzeng, S. Chen, J. Wu, and T.J. Chen. Fuzzy c-means clustering with spatial information for image segmentation. *Computerized Medical Imaging and Graphics*, 30(1):9–15, 2006.
- [14] J. G. Daugman. Uncertainty relation for resolution in space, spatial frequency, and orientation optimized by two-dimensional visual cortical filters. *Optical Society of America A: Optics, Image Science, and Vision*, 2(7):1160–1169, 1985.
- [15] E. R. Davies. *Machine Vision*. San Diego: Academic Press, 1997.
- [16] M. de Bruijne, B. van Ginneken, W. Bartels, M.J. van der Laan, J.D. Blankensteijn, W.J. Niessen, and M.A. Viergever. Automated segmentation of abdominal aortic aneurysms in multi-spectral MR images. In *Proceeding of International Conference on Medical Image Computing and Computer-Assisted Intervention*, pages 538–545, 2003.
- [17] F. Ding, W. K. Leow, and S.-C. Wang. Segmentation of 3D CT volume images using a single 2D atlas. In *Proceeding of International Workshop on Computer Vision for Biomedical Image Applications*, pages 459–468, 2005.
- [18] J. Egmont-Petersen, A. F. Frangi, W. J. Niessen, P.C.W. Hogendoorn, J. L. Bloem, M. A. Viergever, and J.H.C. Reiber. Segmentation of bone tumor in MR perfusion images using neural networks and multiscale pharmacokinetic features. In *Proceedings of International Conference on Pattern Recognition*, volume 4, pages 80–83, 2000.

- [19] S. Eiho, H. Sekiguchi, N. Sugimoto, T. Hanakawa, and Urayama S. Branch-based region growing method for blood vessel segmentation. In *Proceedings of Conference on International Society for Photogrammetry and Remote Sensing*, pages 796–801, 2004.
- [20] J. Feng, H.H.S. Ip, and S.H. Cheng. A 3D geometric deformable model for tubular structure segmentation. In *Proceeding of Multimedia Modelling Conference*, pages 174–180, 2004.
- [21] C. Florin, R. Moreau-Gobard, and J. Williams. Automatic heart peripheral vessels segmentation based on a normal MIP ray casting technique. In *Proceeding of International Conference on Medical Image Computing and Computer-Assisted Intervention*, pages 483–490, 2004.
- [22] M. Franz and R. Schüffny. Segmentation of blood vessels in subtraction angiographic images. In *Proceeding of Conference on Digital Image Computing: Techniques and Applications*, pages 215–224, 2003.
- [23] S. Galic and S. Loncaric. Spatio-temporal image segmentation using optical flow and clustering algorithm. In *Proceeding of International Workshop on Image and Signal Processing and Analysis*, pages 63–68, 2000.
- [24] R. C. Gonzalez and R. E. Woods. *Digital Image Processing*. Prentice Hall, 2002.
- [25] V. Grau, A.U.J. Mewes, M. Alcaniz, R. Kikinis, and S.K. Warfield. Improved watershed transform for medical image segmentation using prior information. *IEEE Transactions on Medical Imaging*, 23(4):447–458, 2004.
- [26] S.R. Gunn and M.S. Nixon. A model based dual active contour. In *Proceedings of the British Machine Vision Conference*, pages 305–314, 1994.
- [27] R.M. Haralick, K. Shanmugam, and I. Dinstein. Textural features for image classification. *IEEE Transactions on Systems, Man, and Cybernetics*, Smc-3(6):610–621, 1973.
- [28] K. Haris, S.N. Efstratiadis, N. Maglaveras, and A.K. Katsaggelos. Hybrid image segmentation using watersheds and fast region merging. *IEEE Transactions on Image Processing*, 7(12):1684–1699, 1998.
- [29] M.S. Hassouna and A.A. Farag. Stochastic segmentation of blood vessels from time-of-flight. In *Proceeding of IEEE International Conference on Image Processing*, volume 1, pages 29–32, 2005.

- [30] W.E. Higgins, W.J.T. Spyra, and E.L. Ritman. Automatic extraction of the arterial tree from 3-D angiograms. In *Proceedings of Conference of the IEEE Engineering in Medicine and Biology Society*, volume 2, pages 563–564, 1989.
- [31] A. Hoover, V. Kouznetsova, and M. Goldbaum. Locating blood vessels in retinal images by piecewise threshold probing of a matched filter response. *IEEE Transactions on Medical Imaging*, 19(3):203–210, 2000.
- [32] I.A. Hunter, J.J. Soraghan, and T. McDonagh. Fully automatic left ventricular boundary extraction in echocardiographic images. *IEEE Computers in Cardiology*, pages 741–744, 1995.
- [33] D. Ilea, O. Ghita, K. Robinson, R. Sadleir, M. Lynch, D. Brennan, and P. F. Whelan. Identification of body fat tissues in MRI data. In *Proceeding of International Conference On Optimization of Electrical and Electronic Equipment*, 2004.
- [34] L.A. Johnson, J.D. Pearlman, C.A. Miller, T.I. Young, and K.R. Thulborn. MR quantification of cerebral ventricular volume using a semiautomated algorithm. *American journal of neuroradiology*, 14:1313–1378, 1993.
- [35] M. Kalinin, D.S. Raicu, J. D. Furst, and D.S. Channin. A classification approach for anatomical regions segmentation. In *Proceeding of IEEE International Conference on Image Processing*, volume 2, pages 1262–1265, 2005.
- [36] M. Kass, A. Witkin, and D. Terzopoulos. Snakes: Active contour models. *International Journal of Computer Vision*, 1(4):321–331, 1987.
- [37] S. Kirkpatrick. Optimization by simulated annealing. *Science*, 220:671–680, 1983.
- [38] C. Kirbas and F. Quek. A review of vessel extraction techniques and algorithms. *ACM Computing Survey*, 36(2):81–121, 2004.
- [39] C. Kirbas and F.K.H. Quek. Vessel extraction in medical images by 3D wave propagation and traceback. In *Proceedings of Third IEEE Symposium on Bioinformatics and Bioengineering*, pages 174–181, 2003.
- [40] J. Kittler, J. Illingworth, and J. Foglein. Threshold based on a simple image statistics. *Computer Vision, Graphics, and Image Processing*, 30:125–147, 1985.

- [41] A. Klein, T.K. Egglin, J.S. Pollak, F. Lee, and A.A. Amini. Identifying vascular features with orientation specific filters and B-spline snakes. *IEEE Computers in Cardiology*, pages 113–116, 1994.
- [42] C. Lacoste, G. Finet, and I.E. Magnin. Coronary tree extraction from x-ray angiograms using marked point processes. In *Proceeding of IEEE International Symposium on Biomedical Imaging: Macro to Nano*, 2006.
- [43] W.E. Lorensen and H.E. Cline. Marching cubes: a high resolution 3D surface reconstruction algorithm. volume 21, pages 163–169, 1987.
- [44] V. Luboz, X. Wu, K. Krissian, C.-F. Westin, R. Kikinis, S. Cotin, and S. Dawson. A segmentation and reconstruction technique for 3D vascular structures. In *Proceeding of International Conference on Medical Image Computing and Computer-Assisted Intervention*, pages 43–50, 2005.
- [45] R. Malladi and J.A. Sethian. An $O(N \log N)$ algorithm for shape modeling. In *Proceeding of the National Academy of Sciences*, pages 9389–9392, 1996.
- [46] M. Mancas and B. Gosselin. Fuzzy tumor segmentation based on iterative watersheds. In *Proceeding of ProRISC (Program for Research on Integrated Systems and Circuits) workshop on Circuits, Systems and Signal Processing*, 2003.
- [47] F. Miles and A. Nutall. Matched filter estimation of serial blood vessel diameters from video images. *IEEE Transactions on Medical Imaging*, 12(2):147–152, 1993.
- [48] I. Mitchell. <http://www.cs.ubc.ca/~mitchell/ToolboxLS/>.
- [49] A. Mitiche and J.K. Aggarwal. Image segmentation by conventional and information-integrating techniques: a synopsis. *Image and Vision Computing*, 3(2):50–62, 1985.
- [50] C. Molina, G. P. Prause, P. Radeva, and M. Sonka. 3-D catheter path reconstruction from biplane angiography using 3D snakes. In *Proceeding of the International Society for Optical Engineering, Medical Imaging*, volume 3338, pages 504–512, 1998.
- [51] D. Nain, A.J. Yezzi, and G. Turk. Vessel segmentation using a shape driven flow. In *Proceeding of International Conference on Medical Image Computing and Computer-Assisted Intervention*, pages 51–59, 2004.

- [52] R. Nekovei and Y. Sun. Back-propagation network and its configuration for blood vessel detection in angiograms. *IEEE Transactions on Neural Networks*, 6:64–72, 1995.
- [53] S. Osher and J.A. Sethian. Fronts propagating with curvature-dependent speed: Algorithms based on Hamilton-Jacobi formulations. *Journal of Computational Physics*, 79:12–49, 1988.
- [54] J. Pan and M. Li. Segmentation of MR osteosarcoma images. In *Proceeding of International Conference on Computational Intelligence and Multimedia Applications*, pages 379–384, 2003.
- [55] A. Papoulis. *Probability, Random Variables, and Stochastic Processes*. McGraw-Hill, 1984.
- [56] C. Pellet, A. Herment, M. Sigelle, P. Horain, H. Maitre, and P. Peronneau. A 3D reconstruction of vascular structures from two X-ray angiograms using an adapted simulated annealing algorithm. *IEEE Transactions on Medical Imaging*, 13:48–60, 1994.
- [57] R. Pohle and K.D. Toennies. Segmentation of medical images using adaptive region growing. In *Proceedings of International Conference on Computer Graphics and Interactive Techniques, Computer Graphics*, volume 4322, pages 1337–1346, 2001.
- [58] C. Pollo, M. B. Cuadra, O. Cuisenaire, J.G. Villemure, and J.P. Thiran. Segmentation of brain structures in presence of a space-occupying lesion. *Neuroimage*, 24(4):990–996, 2005.
- [59] Z. Qian, D. N. Metaxas, and L. Axel. A learning framework for the automatic and accurate segmentation of cardiac tagged MRI images. In *Proceeding of ICCV workshop on Computer Vision for Biomedical Image Applications*, pages 93–102, 2005.
- [60] A. Quddus, P. Fieguth, and O. Basir. Adaboost and support vector machines for white matter lesion segmentation in MR images. In *Proceeding of Engineering in Medicine and Biology Society*, pages 463–466, 2005.
- [61] F.K.H. Quek and C. Kirbas. Simulated wave propagation and traceback in vascular extraction. In *Proceedings of International Workshop on Medical Imaging and Augmented Reality*, pages 229–234, 2001.
- [62] A. Rao and D. Gillies. Vortex segmentation from cardiac MR 2D velocity images using region growing about vortex centres. In *Medical Imaging and Augmented Reality*, pages 222–225, 2001.

- [63] D. Rueckert and P. Burger. Contour fitting using stochastic and probabilistic relaxation for Cine MR images. In *Computer Assisted Radiology*, pages 137–142, 1995.
- [64] Y. Sato, S. Nakajima, H. Atsumi, T. Koller, G. Gerig, S. Yoshida, and R. Kikinis. 3D multi-scale line filter for segmentation and visualization of curvilinear structures in medical images. In *Proceedings of the First Joint Conference on Computer Vision, Virtual Reality and Robotics in Medicine and Medial Robotics and Computer-Assisted Surgery*, pages 213–222, 1997.
- [65] H. Schmitt, M. Grass, V. Rasche, O. Schramm, S. Haehnel, and K. Sartor. An X-ray-based method for the determination of the contrast agent propagation in 3-D vessel structures. *IEEE Transactions on Medical Imaging*, 21:251–262, 2002.
- [66] J. A. Sethian. *Level Set Methods*. Cambridge University Press, 1996.
- [67] J.A. Sethian. *Level Set Methods and Fast Marching Methods*. Cambridge University Press, 1999.
- [68] R. Shojaii, J. Alirezaie, and P. Babyn. Automatic lung segmentation in CT images using watershed transform. *IEEE International Conference on Image Processing*, 2:1270–1273, 2005.
- [69] J. Sijbers, P. Scheunders, M. Verhoye, A. van der Linden, D. van Dyck, and E. Raman. Watershed-based segmentation of 3D MR data for volume quantization. *Journal of Magnetic Resonance Imaging : JMRI*, 15(6):679–688, 1997.
- [70] J. V. B. Soares, J. J. G. Leandro, R. M. Cesar, H. F. Jelinek, and M. J. Cree. Retinal vessel segmentation using the 2-D Morlet wavelet and supervised classification. 2005.
- [71] J.Q. Song, M. Cai, and M.R. Lyu. Edge color distribution transform: An efficient tool for object detection in images. In *Proceedings of International Conference on Pattern Recognition*, volume 1, pages 608–611, 2002.
- [72] M. Sonka, V. Hlavac, and R. Boyle. *Image Processing, Analysis and Machine Vision*. Brooks/Cole Publishing Company, 1999.
- [73] J. Tschirren, E.A. Hoffman, G. McLennan, and M. Sonka. Intrathoracic airway trees: segmentation and airway morphology analysis from low-dose CT scans. *IEEE Transactions on Medical Imaging*, 24:1529–1539, 2005.

- [74] Z. Wu and R. Leahy. A new unsupervised hierarchical segmentation algorithm for textured images. In *Proceeding of International Conference on Acoustics, Speech, and Signal Processing*, pages 2325–2328, 1990.
- [75] C. Xu and J. Prince. Gradient vector flow deformable models. In *Handbook of Medical Imaging*. Academic Press, 2000.
- [76] C. Xu and J.L. Prince. Snakes, shapes, and gradient vector flow. *IEEE Transactions on Image Processing*, 7:359–369, 1998.
- [77] P. Yan and A.A. Kassim. MRA image segmentation with capillary active contour. In *Proceeding of International Conference on Medical Image Computing and Computer-Assisted Intervention*, pages 51–58, 2005.
- [78] A.J. Yezzi, S. Kichenassamy, A. Kumar, P. Olver, and A. Tannenbaum. A geometric snake model for segmentation of medical imagery. *IEEE Transactions on Medical Imaging*, 16(2):199–209, 1997.
- [79] P.J. Yim, P.L. Choyke, and R.M. Summers. Gray-scale skeletonization of small vessels in magnetic resonance angiography. *IEEE Transactions on Medical Imaging*, 19:568–576, 2000.
- [80] R. J. Zawadzki, A. R. Fuller, M. Zhao, D. F. Wiley, S. Choi, B. A. Bower, B. H., J. A. Izatt, and J. S. Werner. 3D OCT imaging in clinical settings: Toward quantitative measurements of retinal structures. In *Proceeding of Photonics West – Electronic Imaging 2006*, volume 6138, pages 8–18, 2006.